Investigation of transitional turbulence models for CFD simulation of the drag crisis for flow over a sphere

IOP Conf. Series: Materials Science and Engineering **700** (2019) 012007 doi:10.1088/1757-899X/700/1/012007

Investigation of transitional turbulence models for CFD simulation of the drag crisis for flow over a sphere

S M Nakhostin and K E T Giljarhus*

Department of Mechanical and Structural Engineering and Materials Science, University of Stavanger, Stavanger, Norway

* Corresponding author: knut.e.giljarhus@uis.no

Abstract. The drag crisis is an interesting physical phenomenon for flow over bluff bodies, where the drag coefficient suddenly drops as the Reynolds number increases. This behavior is caused by the flow transitioning from laminar to turbulent flow in the boundary layer. The turbulent flow remains attached to the surface longer than the laminar flow, thereby reducing the size of the wake behind the body. The phenomenon has been extensively studied experimentally for simple geometries such as flow over a sphere or a cylinder. Numerical simulations, however, have mainly been performed in either the subcritical or the supercritical region. In this study, we investigate the ability of steady-state RANS CFD models to predict the drag crisis for flow around a sphere. Experiments using oil-film visualization are performed to determine the type of transition for flow over a sphere. Simulations are performed using OpenFOAM, with the k-ω shear stress transport (SST) turbulence model. For transition modelling, the Langtry-Menter modification to the SST model is considered. The simulations show improved prediction of the drag coefficient in the subcritical regime, but the implementation of the model is found to be unstable in the critical and supercritical range.

1. Introduction

The boundary conditions applied to solid surfaces in industrial CFD (computational fluid dynamics) simulations are typically assuming a fully turbulent boundary layer. This is often sufficient since relevant conditions for engineering-type structures typically are such that the boundary layer is turbulent for most of the structure. However, there are several cases in e.g. aerospace, wind turbines and turbomachinery where the transition from laminar to turbulent flow in the boundary layer can be relevant. Failing to account for the transition can lead to erroneous prediction of engineering quantities such as heat transfer coefficients and skin friction coefficients.

For flow in a boundary layer, the phenomena leading to transition are typically divided into three different modes; bypass transition, natural transition and separation-induced transition. Bypass transition is caused by turbulence from the free stream diffuses into the boundary layer, generating disturbances that eventually lead to transition. Natural transition is only possible for very smooth walls and extremely low disturbances in the mean flow. Here, initial disturbances develop into streamwise, unstable waves called Tollmien-Schlitling waves. The growth and breakdown of these waves eventually lead to a fully turbulent flow. Separation-induced transition typically occur in adverse pressure gradient flows where the laminar boundary layers separates, causing turbulence to be generated in the shear layer and subsequent turbulent reattachment.

Transition is a complex physical phenomenon and transition modelling is still an active area of research. No model has yet reached the level of maturity necessary for routine engineering simulations. The most popular turbulence models used in engineering are RANS (Reynolds-Averaged Navier-Stokes) models, which simulate the average flow field and account for turbulence by adding an additional turbulent viscosity to the Navier-Stokes equations. In the pioneering work of [1], the so-called local correlation-based transition model (LCTM) concept was introduced for transition modelling. These models attempt to solve additional transport equations to give a local criterion for transition. Hence, instead of modelling the physics of transition, they rely on empirical correlations to model the behavior. These models are suitable for implementation into a RANS framework and is therefore promising for use in general-purpose CFD simulations. Recently, a review of transition models based on LCTM showed good agreement for a wide range of test cases [2].

Most simulations with transition models have been performed on streamlined structures such as turbine blades, airfoils and wing turbines. Bluff bodies, characterized by large adverse pressure gradients and significant regions of separated flows, have been comparatively less studies in the context of transition modelling. Transition effects can have a crucial effect on such structures. A well-known phenomenon is the drag crisis, where the drag coefficient suddenly drops as the Reynolds number increases. This phenomenon can in some cases be exploited to create more efficient designs. The classical example is the dimples applied to a golf ball, which makes the ball fly longer due to initiating the drag crisis at a lower Reynolds number [3].

This study is an initial study of the capability of transition models to capture the drag crisis for flow over a sphere. The flow over a sphere is a fundamental problem in fluid dynamics, and has been studied extensively in the literature. A thorough review was recently performed in [4, 5]. Experimentally, the full range of Reynolds numbers have been studied. Most recently, the existence of a laminar separation bubble was found in the supercritical region [6]. When it comes to numerical methods, the lower range of Reynolds numbers before transition has been studied by several authors with good results. A few studies have been made in the super-critical regime [7-9]. Notably, only a single study has been performed in the drag crisis range [10]. This was done using a high-order Lattice-Boltzmann method, without applying any sub-grid turbulence model or wall model. Even with large unstructured grids with more than 100 million grid cells, they do not resolve the boundary layer completely, but their results indicate that the drag crisis can be reproduced by numerical simulations. Since such direct simulation methods are unsuitable for most engineering-type simulations, this study investigates the ability of steady-state RANS methods with transition modelling to reproduce the drag crisis phenomenon. The CFD simulations are performed with the open source CFD software OpenFOAM. Additionally, experiments using oil-film visualization are performed to see if the results from [6] could be reproduced and to obtain further insight into the transition behavior.

Section 2 introduces the numerical model and the transition turbulence model. Next, Section 3 describes the computational setup with details on the computational mesh and numerical settings. Sections 4 provides information on the experimental setup. Section 5 presents and discusses the results, while in Section 6 conclusions are drawn and recommendations for further work proposed.

2. Numerical model

The numerical model is based on the steady-state Reynolds-Averaged Navier-Stokes equations,

$$\frac{\partial u_i}{\partial x_i} = 0 \tag{1}$$

$$u_j \frac{\partial u_i}{\partial x_j} = -\frac{1}{\rho}\frac{\partial P}{\partial x_i} + \nu \frac{\partial^2 u_i}{\partial x_j^2} - \frac{\partial \overline{u_i' u_j'}}{\partial x_j} \tag{2}$$

Here, u_i represents the averaged velocity components, P is the dynamic pressure, ρ is the density and ν the kinematic viscosity. The influence of turbulence is accounted for by the Reynolds stress tensor, $\overline{u_i' u_j'}$. Here, u_i' denotes the fluctuating part of the velocity. The Reynolds stress component is modelled using the Boussinesq approximation, where it is expressed in terms of a turbulent viscosity, ν_t, and the mean flow gradients,

$$-\overline{u_i' u_j'} = \nu_T \left(\frac{\partial u_i}{\partial x_j} + \frac{\partial u_j}{\partial x_i} \right) - \frac{2}{3} k \delta_{ij} \tag{3}$$

Here, k is the turbulent kinetic energy and δ_{ij} is the Kronecker delta function. The k-ω SST turbulence model is used to find the turbulent viscosity [11].

The Langtry-Menter model is used to model transition. This model is an addition to the k-**ω** SST model. The model does not attempt to model the actual physics of the transition process, but instead couples the general turbulence model with correlation-based transition modeling. Since the model contains a large number of correlations, only a brief overview of the model is given here, more details can be found in [1]. The model is also known as the γ-$Re_{\theta t}$ –SST model, because it makes use of two additional variables; the intermittency, γ, and the transition momentum thickness Reynolds number, $Re_{\theta t}$, in addition to the k and ω equations. The intermittency value is used to trigger the transition locally. It is coupled with the production of turbulent kinetic energy and used to turn on production downstream of the transition. The transition momentum thickness Reynolds number is used to capture the effect of the freestream behavior on the boundary layer. The two extra equations for $Re_{\theta t}$ and γ that are solved in this model are

$$\frac{\partial(\rho\gamma u_j)}{\partial x_j} = P_\gamma - E_\gamma + \frac{\partial}{\partial x_j} \left[\left(\mu + \frac{\mu_t}{\sigma_f} \right) \frac{\partial \gamma}{\partial x_j} \right] \tag{4}$$

$$\frac{\partial(\rho u_j Re_{\theta t})}{\partial x_j} = P_{\theta t}(Re_{\theta t0} - Re_{\theta t}) + \frac{\partial}{\partial x_j} \left[\sigma_{\theta t}(\mu + \mu_t) \frac{\partial Re_{\theta t}}{\partial x_j} \right] \tag{5}$$

The production term in the intermittency equation is designed to be switched on whenever the local strain rate exceeds the transition criteria. It contains multiple correlations that are tuned based on experiments performed of flow over a flat plate. The sink term ensures that the intermittency is close to zero in the laminar boundary layer and can also be used to model relaminarization. The equation for $Re_{\theta t}$ is used to transfer information from the free-stream to the boundary layer to give a local criterion for transition. The production term in this equation contains a correlation for the transition onset based on experiments.

The only modification to the SST model is that the production and dissipation terms in the equation for turbulent kinetic energy now include the intermittency to control the production/dissipation as follows,

$$\overline{P_k} = \gamma P_k$$

$$\overline{D_k} = \min(\max(\gamma, 0.1), 1.0)\, D_k$$

3. Computational setup

The above numerical model is solved using the OpenFOAM toolbox, version 6.0. The computational domain has size 20D x 10D x 10D, where D is the sphere diameter. The sphere is placed 5D from the inlet. At the inlet, constant inlet values as used, with a turbulence intensity of 0.5 %, and zero gradient for pressure. At the outlet, constant pressure is set with zero gradient for the remaining variables. Slip conditions are used at the sides of the domain.

The computational mesh is generated using the snappyHexMesh mesh generator. Three levels of refinement are used in the wake region and around the sphere, and layers are added near the surface to obtain a sufficiently fine resolution in the boundary layer. Around 20-30 cells are used in the layer

region, with a stretching factor of 1.2. The y+ value was less than 1 for all cases. Figure 1 shows the overall mesh as well as a close-up of the mesh near the sphere surface.

The discretization scheme used for the convective term is the limited linear scheme, which is a central-upwind scheme using the Sweby limiter. For the remaining Laplacian, gradient and surface normal gradient terms the linear schemes are used, which apply the Gauss divergence theorem with explicit non-orthogonal correction. The SIMPLE algorithm is used for pressure-velocity coupling and the iteration procedure is stopped when the drag coefficient has converged to four significant digits.

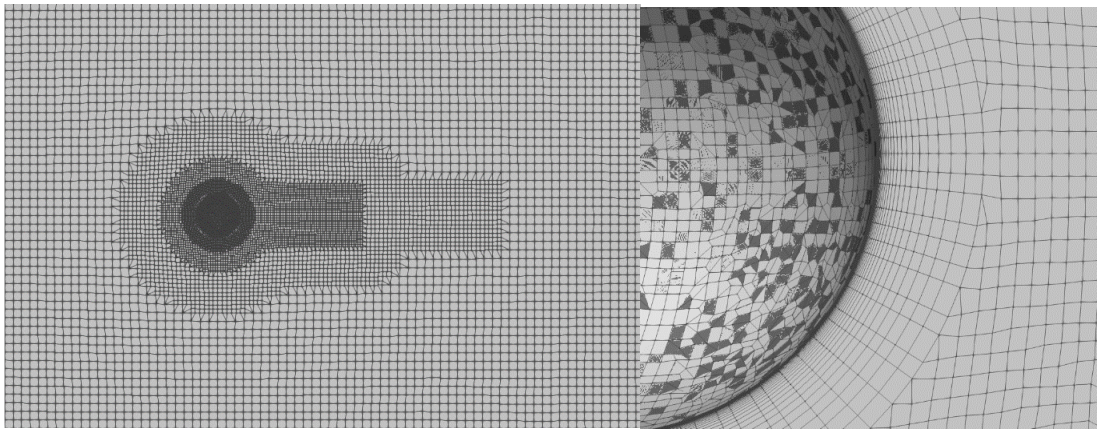

Figure 1. Illustration of computational mesh (left) and close-up of layers near the surface (right).

3.1. Mesh convergence study

To determine the sufficient size of the computational mesh, a mesh convergence study was performed for the case with Reynolds number 5×10^5. For the convergence study, the distance to the first cell is kept constant to maintain $y^+ = 1$ and the overall grid resolution elsewhere is increased**.** Figure 2 shows the drag coefficient for four grid sizes. For the two last grids, the coefficient converges to the value of 0.166. Hence, the grid size of approximately 500 000 cells is found to be sufficient for Reynolds number 5×10^5. For the sake of simplicity, this resolution is kept for all cases and only the distance to the first cell and number of cells in the near-wall layer is modified for the remaining cases.

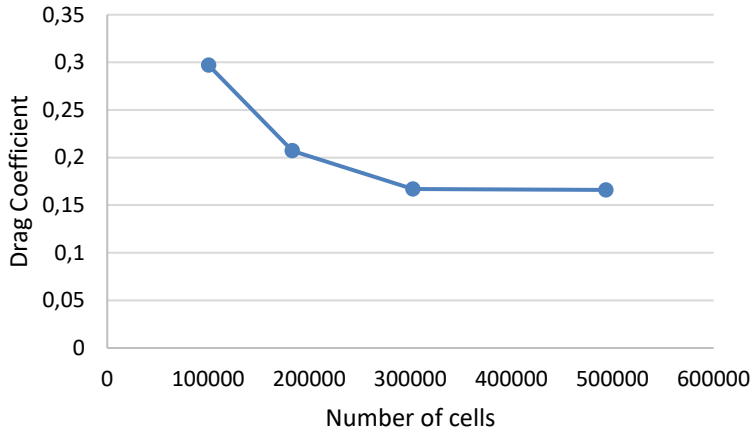

Figure 2. Mesh convergence study.

4. Experimental setup

The experiments were performed at the fluid mechanics lab at the Norwegian University of Science and Technology in Trondheim, Norway. A sphere with diameter 170 mm was placed in a closed-circuit wind tunnel with test section dimensions 1 m by 0.5 m. The wind tunnel is capable of speeds up to 35 m/s at

low turbulence intensities of approximately 0.2 %. .The sphere was placed on a rod with 19 mm diameter, and with 130 mm distance from sphere to the floor of the wind tunnel. The setup is shown in Figure 3. The rod is connected to a force balance to measure the forces on the geometry. Note that since the rod is relatively thick compared to the sphere, and placed under the sphere, the rod will significantly influence the drag and the force results will not be directly comparable to other results in the literature. To investigate the transition behaviour, the sphere was covered in a mixture of motor oil and canola oil mixed with white dry pigment.

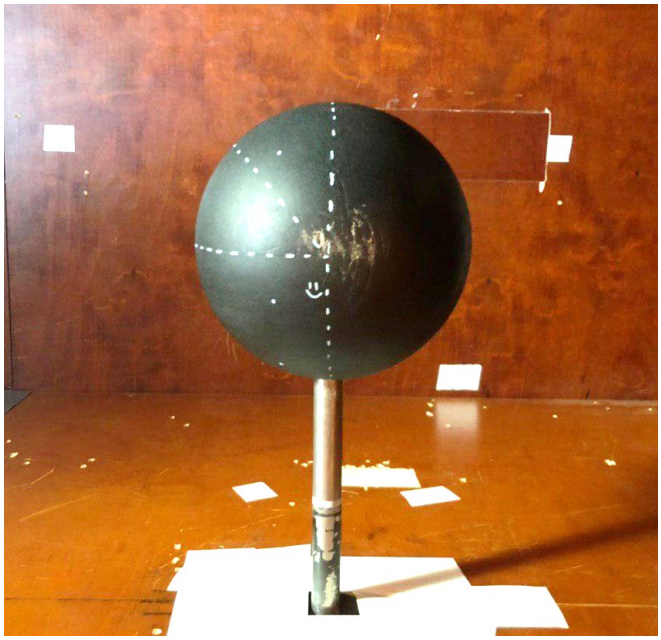

Figure 3. Sphere placed in wind tunnel.

5. Results

The experimental results are summarized in Figure 4. The drop in drag coefficient can be clearly seen at a Reynolds number of approximately 2.8×10^5. The oil film visualization for a Reynolds number of 3.2×10^5 illustrates the transition and separation behaviour. At the first line, there is laminar separation from the sphere, causing a laminar separation bubble. At the second line, there is turbulent reattachment before the flow finally fully separates from the sphere at the third line. This is in agreement with the results from [6]. In the development of the Langry-Menter transition model [1], the model is compared against several flat-plate test cases, both with zero pressure gradient and non-zero pressure gradients. Only one of these cases, T3C4, is designed to test separation-induced transition. In [1], they report good agreement for the skin friction for this case, but in [12], it is shown that for the Reynolds shear stress and turbulence kinetic energy, the results are rather unsatisfactory.

Figure 5 compares the simulated drag coefficients with the experiments of [13] and the empirical correlation from [14]. In the subcritical region, there is good agreement between the experiments and the simulations. However, in the transition region, the fully turbulent model deviate significantly from the experiments. This is expected, as for the fully turbulent model, the turbulent boundary layer will lead to later separation and thereby smaller wake and pressure drag. In the supercritical region, however, the results are in reasonable agreement with the experiments again. The transition model gives better agreement to the experiment in the transition region, but the deviation is still significant. Unfortunately, the simulations for higher Reynolds numbers with the transition model showed numerical instabilities so they are not included here.

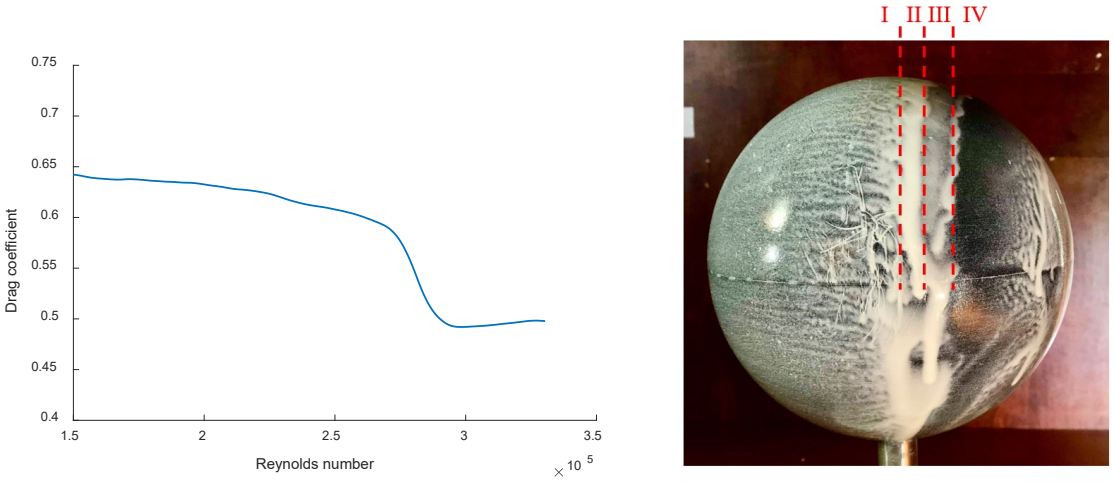

Figure 4. Experimental results. Left: Drag coefficients. Right: Oil film visualization of flow over sphere after drag crisis. I: Laminar boundary layer. II: Laminar separation bubble. III: Turbulent reattachment. IV: Turbulent separation.

Figure 6 show contours of velocity for the two turbulent models at $\mathrm{Re} = 1 \times 10^5$. The fully turbulent model has a smaller wake area than the transition model which explains the difference in drag values. This effect is further illustrated in Figure 7, which shows the pressure coefficient along the sphere surface. The simulation values are compared against the experiments of [13]. The experiment at $\mathrm{Re} = 1.62 \times 10^5$ are in the subcritical range while the experiment at $\mathrm{Re} = 3.18 \times 10^5$ are in the supercritical range. The fully turbulent simulation agree well with the pressure in the supercritical range. The transitional model is slightly closer to the subcritical pressure, but there are still significant differences. This corresponds to the discrepancies observed for the drag coefficient values.

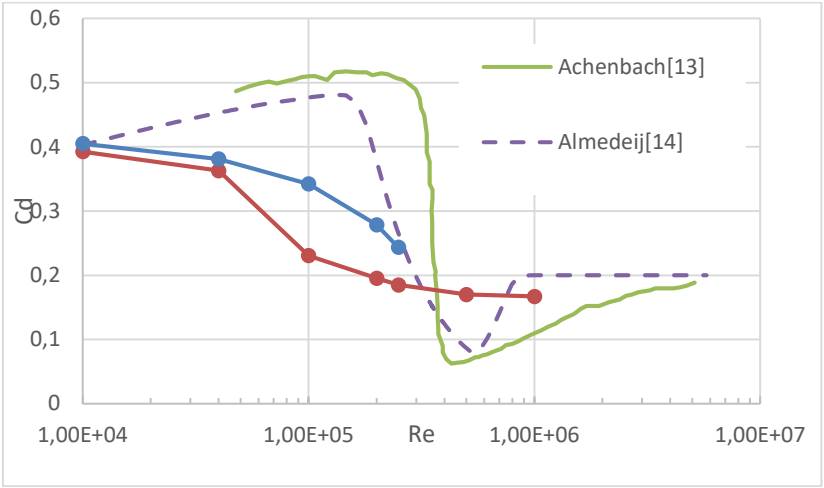

Figure 5. Comparison of experimental results of Achenbach [13], empirical relationship of Almedeij [14] and numerical results of this work with and without transition model.

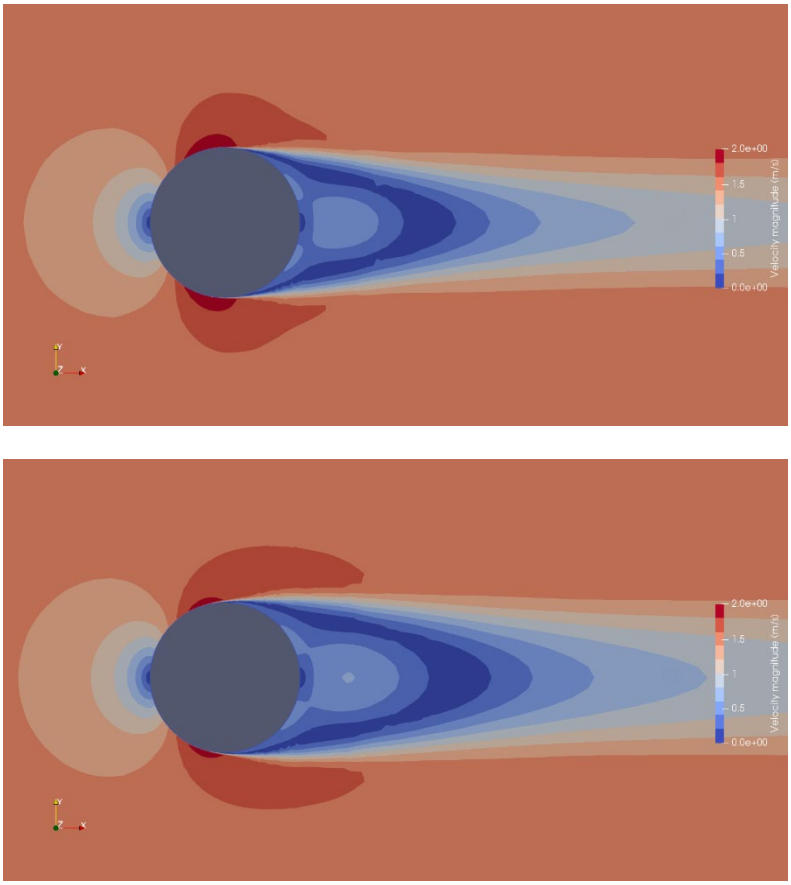

Figure 6. Comparison of velocity magnitude for $\mathrm{Re} = 1 \times 10^5$ for fully turbulent model (top) and transition model (bottom).

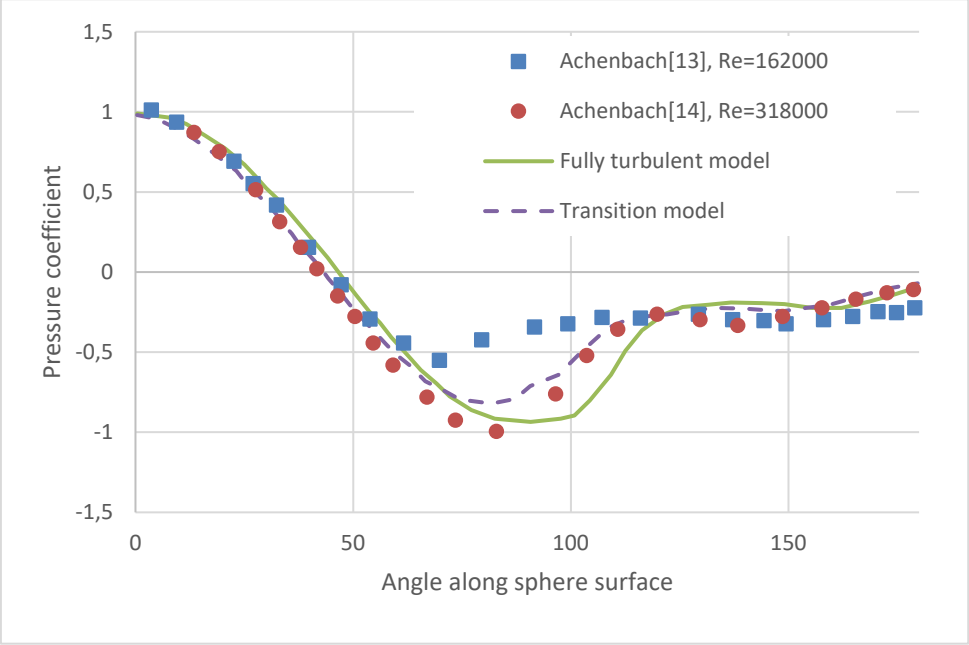

Figure 7. Pressure coefficient along sphere surface. Comparison of fully turbulent and transition model with experimental data from Achenbach[13].

6. Conclusions

In this study, we investigated the ability of CFD models to predict the drag crisis for flow around a sphere. Simulations were performed using the k-**ω** SST model with the Langtry-Menter transition model. Experiments using oil-film visualization were performed to determine the type of transition for flow over a sphere. The experiment showed the existence of a laminar separation bubble, with subsequent turbulent reattachment and separation. This is in agreement with recent experiments performed in [6]. The simulations showed improved prediction of the drag coefficient in the subcritical regime, but still with significant errors compared to the experiments. Due to numerical instabilities at higher Reynolds numbers, the model could not be applied to the critical Reynolds number range.
Future work will perform more experiments in the subcritical range, as well as investigate the numerical instabilities in more detail. Additionally, newer transition models such as the fully algebraic model introduced in [15] will be implemented in OpenFOAM and applied to this problem.

Acknowledgments

We thank Lars Morten Bardal and Ola Elfmark at SIAT – Centre for Sports Facilities and Technology for their kind assistance with the wind tunnel experiments.

References

[1] Menter F R, Langtry R and Völker S 2006 Transition modelling for general purpose CFD codes, *Flow turbul. combust*. **77**(1-4) 277-303
[2] Kaynak U, Bas O, Cakmakcioglu S C and Tuncer I H 2019 Transition Modeling for Low to High Speed Boundary Layer Flows with CFD Applications *In Boundary Layer Flows-Theory, Applications and Numerical Methods.* DOI: 10.5772/intechopen.83520
[3] Bearman P W and Harvey J K 1976 Golf ball aerodynamics *Aeronaut. Quart.* **27**(2) 112-122
[4] Tiwari S S, Pal E, Bale S, Minocha N, Patwardhan A W, Nandakumar K and Joshi J B 2019 Flow past a single stationary sphere, 1. Experimental and numerical techniques, *Powder Technol.*
[5] Tiwari S S, Pal E, Bale S, Minocha N, Patwardhan A W, Nandakumar K and Joshi J B 2019 Flow past a single stationary sphere, 2. Regime mapping and effect of external disturbances, *Powder Technol.,* In Press
[6] Deshpande R, Kanti V, Desai A and Mittal S 2017 Intermittency of laminar separation bubble on a sphere during drag crisis, *J. Fluid Mech.* **812** 815-840
[7] Constantinescu G and Squires K 2004 Numerical investigations of flow over a sphere in the subcritical and supercritical regimes, *Phys. Fluids* **16** 1449–66
[8] Jindal S, Long L, Plassmann P and Uzol N 2004 Large eddy simulations around a sphere using unstructured grids, *In 34th AIAA Fluid Dyn Conf Exhib*
[9] Jones D A and Clarke D B 2008 Simulation of flow past a sphere using the fluent code ADA494935
[10] Geier M, Pasquali A and Schönherr M 2017 Parametrization of the cumulant lattice Boltzmann method for fourth order accurate diffusion Part II: Application to flow around a sphere at drag crisis, *J. Comput. Phys.* **348** 889-98
[11] Menter F R, Kuntz M and Langtry R 2003 Ten years of industrial experience with the SST turbulence model *In Proc. fourth int. symp. Turbu., heat and mass transfer* 625–632
[12] Suluksna K, Dechaumphai P and Juntasaro E 2009 Correlations for modeling transitional boundary layers under influences of freestream turbulence and pressure gradient, *Int. J. Heat Fluid Flow* **30**(1) 66-75
[13] Achenbach E 1972 Experiments on the flow past spheres at very high Reynolds numbers, *J. Fluid Mech.* **54**(3) 565-75
[14] Almedeij J 2008 Drag coefficient of flow around a sphere: Matching asymptotically the wide trend, *Powder Technol.* **186**(3) 218-23
[15] Cakmakcioglu SC, Bas O, Kaynak U 2018 A correlation-based algebraic transition model, *Proc. Ints. Mech. Eng. C-J. Mech. Eng. Sci.* **232**(21) 3915-29